NASA-CR-197299

39796
O CIT. 16P

RSS Tech. Memo. 010395 Issued: January 3, 1995

Progress Report for Contract NASW-4714

August 1993 Through January 1995

# Deriving Earth Science Products from SSM/I

Principal Investigator: Frank J. Wentz

N95-20156
Unclas
G3/43 0039796

Prepared for:
Mission to Planet Earth
National Aeronautics and Space Administration
Washington, DC 20546

Prepared by:

Remote Sensing Systems
1101 College Ave., Suite 220, Santa Rosa, CA 95404 (707) 545-2904

(NASA-CR-197299) DERIVING EARTH SCIENCE PRODUCTS FROM SSM/I Progress Report, Aug. 1993 - Jan. 1995 (Remote Sensing Systems) 16 p

# Deriving Earth Science Products from SSM/I
# Progress Report: August 1993 Through January 1995
# Principal Investigator: Frank J. Wentz

## 1. SUMMARY OF PROGRESS

There have been several major accomplishments during the second phase of this investigation:

1. All three SSM/I's (F08, F10, and F11) have been cross-calibrated. Thus it is now possible to produce an 8-year time series (1987-1994) of geophysical products free of inter-satellite biases. The accuracy of the cross-calibration is approximately 0.1 K.

2. A very large, quality-controlled, collocated SSM/I and radiosonde data set has been produced. This data set contains 36,000 SSM/I overpasses of island and ship radiosonde stations. This data set complements the SSM/I-buoy data set that was produced last year.

3. The SSM/I-radiosonde and SSM/I-buoy data sets have been used to calibrate the SSM/I ocean retrieval algorithm. In addition to calibrating the algorithm, a number of other updates were made based on our analysis of the first 5 years of SSM/I products and also based on feedback that we have received from other investigators using our products. The revised algorithm is called SSM/I-2. The SSM/I-2 algorithm is extremely well calibrated. The rms accuracies of the retrieved wind speed, water vapor, and cloud water are approximately 1 m/s, 1 mm, and 0.02 mm, respectively. Systematic errors such as crosstalk between the retrieved parameters have been virtually eliminated. We know of no other SSM/I algorithm that can match this performance.

4. Ocean products have been produced for both the F10 and F11 SSM/I for the 1991 through 1993 period. The new SSM/I-2 algorithm was used to generate these products.

5. A scientific paper entitled "A Well-Calibrated Ocean Algorithm for SSM/I" is near completion. This paper describes the SSM/I-2 algorithm and validation results. The paper will soon be submitted for publication in the refereed scientific literature.

6. The SSM/I-buoy data set was used to better determine the variation of the ocean $T_B$ with wind direction. The results clearly show a significant azimuthal variation in $T_B$. The same wind direction dependence is found in the tropics, mid-latitudes, and poleward latitudes. These results further support the feasibility of using satellite microwave radiometers for measuring wind direction.

7. We have demonstrated that under high wind conditions, wind direction information can be obtained from individual SSM/I observations. Previously, monthly wind directions were obtained by averaging together many SSM/I orbits. The new results suggest that a single-look polarimetric radiometer may be able to measure both wind speed and direction for moderate to high winds. However, a two-look radiometer system is still the preferred option for measuring wind direction under all conditions.

8. The principal investigator, F. Wentz, has participated as a member of four NASA working groups: (1) SSM/I Pathfinder, (2) WetNet, (3) Physical Oceanography DAAC Working Group, and (4) Hydrological DAAC Working Group. He is the leader of the Ocean Group for the SSM/I Pathfinder and is the leader of the Vapor and Clouds Group for WetNet.

We will now describe these activities in more detail.

## 2. CROSS-CALIBRATION OF F08, F10, AND F11 SSM/I's

Considerable effort was spent cross-calibrating the three SSM/I's. For the F08-F10 cross-calibration, we used individual orbit crossovers to obtain near-simultaneous observations. In this way, the error due to the random spatial-temporal variability and due to the diurnal cycle is minimized. An orbit crossover is defined as the overlap region of the F08 and F10 swaths. Two crossovers occur for each complete orbit. The typical time difference between the F08 and F10 observation at the crossover point is 30 minutes. Over the ocean, this time difference has a negligible effect on the comparison statistics. However, over land in the morning, the land temperature is rapidly increasing by about +4 K/hour, thus making a time difference of 30 minutes significant. We therefore did not use morning land crossovers in the intercalibration. For the evening land crossovers, the cooling rate is about −1 K/hour. We applied a first-order correction to compensate for this cooling rate and then used the evening land crossovers in the intercalibration. For the ocean, no cooling or heating in the $T_A$'s was detected, as was expected. All crossovers that occurred during 1991 were used to determined the F08-F10 cross-calibration coefficients.

As a check on the F08-F10 cross-calibration coefficients, the coefficients were calculated in another, simpler way. Monthly, 1° latitude by 1° longitude ocean maps of the F08 and F10 $T_A$'s were first computed. Then these monthly maps were differenced. The coefficients found from this simpler approach agreed with the those found from the more precise orbit crossover analysis to within 0.15 K.

The data flow for F08 stopped in December 1991, and the first data for F11 began in December 1991. There is about 1 week of overlapping F08 and F11 data, which is insufficient to do a cross-calibration. Thus, we are forced to do a serial cross-calibration in which F11 is cross-calibrated to the F10 $T_A$'s that have been adjusted to match the F08 $T_A$'s.

In doing the F10-F11 calibration, we decided not to use the near-simultaneous orbit crossover technique because the geometry of the F10 and F11 orbits is such that the crossovers occur at 80 N and 80 S. Thus, unlike the F08-F10 crossovers, the F11-F10 crossovers do not occur over the unfrozen ocean, but rather occur over sea ice in the north and Antarctica in the south. We felt that it was best to have the intercalibration based on ocean observations. Due to the Earth's rotation the F10 and F11 swaths do cross over again at the lower latitudes, but the time lag for these crossovers is about 3.5 hours. We use these time-lag crossovers for the F10-F11 calibration. The 3.5-hour difference is large enough to make the diurnal cycle a significant source of error in the F10-F11 calibration. We therefore make a correction for the diurnal cycle. The effect of the diurnal cycle is estimated from an analysis of the F08 and F10 $T_A$'s. This estimated diurnal cycle is then removed from the F10-F11 $T_A$ differences.

In order to assess the accuracy of the F10-F11 cross-calibration, we computed the cross-calibration coefficients four different ways:

1. Using just the morning ocean crossovers with a correction for the diurnal cycle.
2. Using just the evening ocean crossovers with a correction for the diurnal cycle.
3. Using both the morning and evening ocean crossovers with no diurnal cycle correction.
4. Using the near simultaneous crossovers in Antarctica

The cross-calibration coefficients obtained from Methods 1 and 2 are very similar (0.1K), which bolsters our confidence in the overall procedure. The assumption in Method 3 is that the effect of the diurnal cycle will tend to cancel out when morning and evening observations are averaged together. The results tend to bare this out. The Method 3 coefficients are within 0.3 K of the Method 1 and 2 values. Method 4 has the advantage of near simultaneous observations (30 minutes), but it has the disadvantage of being over the mountainous snow covered terrain of Antarctica. Except for the 19H channel, the cross-calibration coefficients for Method 4 are within 0.2 K of the Method 1 and Method 2 values. It is very encouraging to obtain such similar results for land and ice observations. However the 19H coefficient found from the Antarctica observations is 0.7 K higher than that found from the ocean observations. The reason for this is unclear. Possibly the fact that the azimuth angle for F10 and F11 differs by 50° at the crossover point is causing the offset.

Before comparing the F08, F10, and F11 $T_A$'s, an adjustment is required to correct for the difference in incidence angle for the various observations. The incidence angle difference is typically about 0.2°. Over land and ice, this difference has a very small effect (less than 0.1 K) on $T_A$, and no correction was made for land or ice. Over the oceans, the difference corresponds to a $T_A$ difference of 0.2 K for horizontal polarization and 0.4 K for vertical polarization. For ocean observations, the $T_A$'s were first normalized to a common incidence angle of 53.25° before doing the intercalibration. The adjustment is based on the standard ocean brightness temperature model.

The F10 minus F08 $T_A$ differences were regressed to the following linear expression.

$$T_{A10} - T_{A08} = A + B\,(T_{A10} + T_{A08})/2$$

The regression coefficients A and B were found for the five lower SSM/I channels. For the F10-F11 cross-calibration, the 3.5 hour time lag is too large to allow for the determination of the B coefficient. Thus we assumed F10 and F11 have the same the B coefficient and just found the F11-F10 $T_A$ offset (i.e., the A coefficient). The A and B coefficients are used to adjust the F10 and F11 $T_A$'s to correspond to the F08 $T_A$'s. The adjustment is the following:

$$\hat{T}_{A10} = (1 - B_{10})T_{A10} - A_{10}$$

$$\hat{T}_{A11} = (1 - B_{11})T_{A11} - A_{11}$$

where $\hat{T}_{A10}$ and $\hat{T}_{A11}$ are the adjusted $T_A$'s for F10 and F11, respectively. Table 1 gives the values for the F10 and F11 A and B coefficients. As can been seen for Table 1, the $T_A$ offsets among the 3 satellites is typical of the order of 0.5 K, which indicates SSM/I is a very well calibrated instrument. The adjusted antenna temperatures are then used in the geophysical

retrieval algorithm to generate products that are free of biases due to the sensor calibration differences among the three satellites.

**Table 1. Cross-Calibration Coefficients for F10 and F11**

| | | | | |
|---|---|---|---|---|
| | 0.08 K | 0.44 K | 0.00221 | 0.00221 |
| | 0.35 K | –0.16 K | 0.00079 | 0.00079 |
| | –0.33 K | 0.30K | 0.00161 | 0.00161 |
| | –0.01 K | -0.01 K | 0.00335 | 0.00335 |
| | 0.44 K | –0.03 K | 0.00165 | 0.00165 |

In addition to the cross-calibration, an alongscan calibration was done for F08, F10, and F11. This calibration removes a systematic error that is a function of the scan position. We think that the systematic error is due to the radiometer horn partially seeing the cold sky reflector at one edge on the Earth-viewing scan segment. This alongscan calibration is essentially the same (0.05 K) for all 3 SSM/I's.

## 3. RADIOSONDE AND BUOY OBSERVATIONS COLLOCATED WITH SSM/I

A very large, quality-controlled, collocated SSM/I and *in situ* data set has been compiled. This data set is used to precisely calibrate the SSM/I ocean algorithm. The two parts of the data set are the collocated SSM/I-buoy observations and the collocated SSM/I-radiosonde observations. After subjecting the *in situ* data to a rigorous quality control procedure, we obtained 45,000 SSM/I overpasses of moored ocean buoys and 36,000 SSM/I overpasses of radiosonde sites on weather ships and small islands. We now describe the methodology for compiling the two data sets.

The buoy data sets were obtained from the following three sources:

1. National Data Buoy Center (NDBC)
2. Pacific Marine Environmental Laboratory (PMEL)
3. Japanese Meteorological Association (JMA)

All available buoy reports from these sources were collected for the 4 year period from 1987 through 1990. NDBC operates about 75 moored buoys and 50 C-man stations located in the Northeast Pacific, in the Gulf of Mexico, in the Northwest Atlantic, near Hawaii, and one off the coast of Peru. Of these, we selected the 42 stations that are at least 30 km from the coast. PMEL distributes the TOGA-TAO buoy data, which is a network of moored buoys in the Equatorial Pacific. For the 1987-1990 period, there are 20 TOGA-TAO mooring sites. And, JMA operates four buoys that are off the coast of Japan. This gives a total of 66 sites, which are shown in Figure 1.

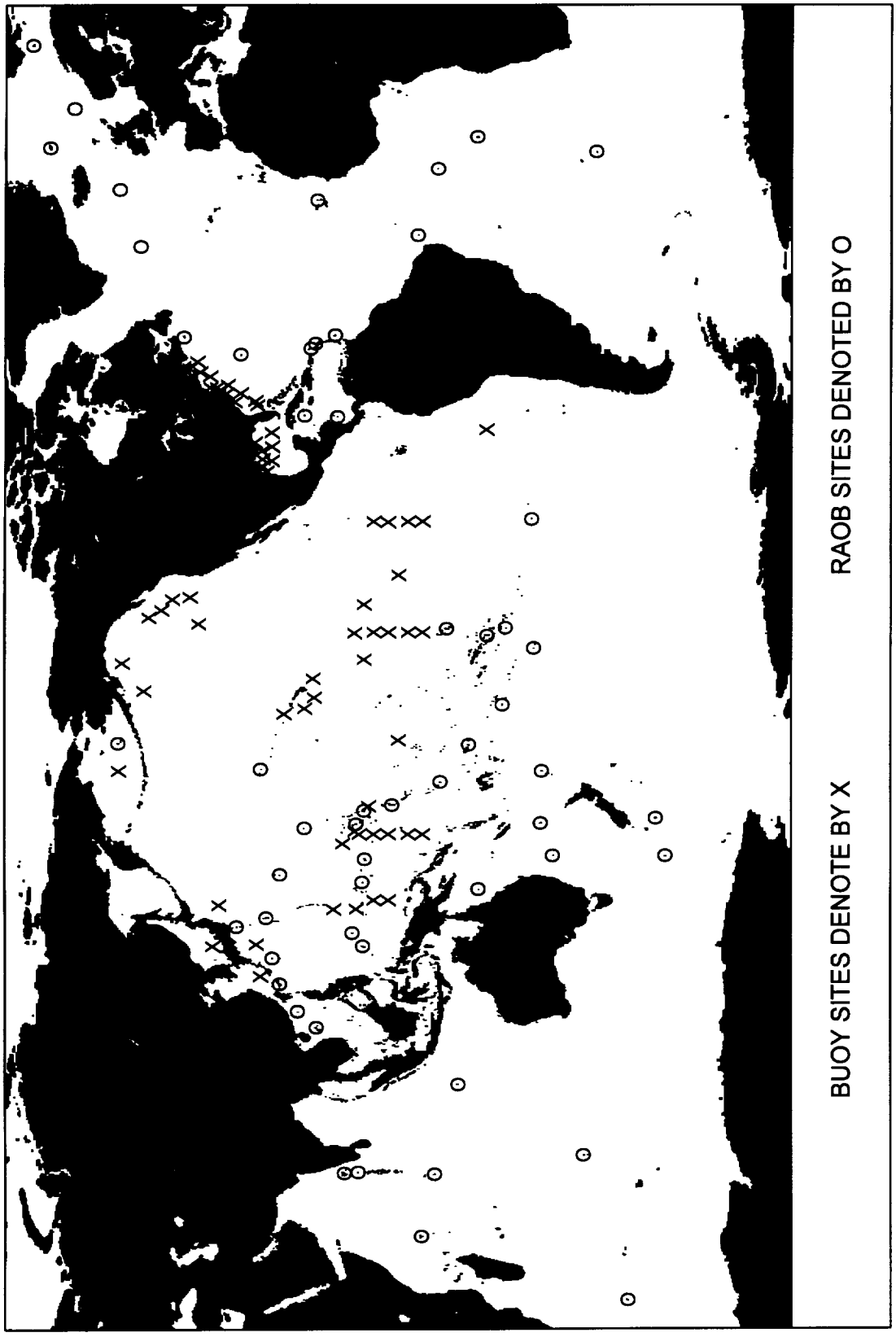


FIG. 1. LOCATION OF BUOY AND RADIOSONDE SITES FOR SSM/I VALIDATION.

The sampling time and interval is different for the various buoy data sets. In general, the NDBC moored buoys are sampled for 8.5 minutes at 1 hour intervals, and the NDBC C-man anemometers are sampled for 2 minutes at 1 hour intervals. The TOGA-TAO buoys take continuous measurements and report the averaged wind at various intervals (1, 2, 6, and 24 hours), depending on the buoy electronics. The JMA buoys sample for 10 minutes at 3 hour intervals.

For each buoy location, a collocation program found all SSM/I overpasses for which any portion of the swath is within 30 km of the buoy. A time interpolation was then done to specify the buoy wind speed at the time of the SSM/I overpass. The buoy observations were subjected to the usual set of quality control procedures, including checks for missing data, blank fields, and out-of-bounds data. In addition, if within the specified time window the winds vary by more than 10 m/s, then the SSM/I overpass was discarded because there is probably too much variation in the wind field for an accurate satellite versus *in situ* comparison.

The radiosonde observations (RAOB) for the 1987 through 1990 period were obtained from the National Center for Atmospheric Research (NCAR). Since the accuracy of the SSM/I retrievals degrade when land is close by, we selected only those radiosonde sites that are on weather ships or on small islands. Figure 1 shows the location of the 55 selected sites.

For each RAOB location, a collocation program found all SSM/I overpasses for which any portion of the swath is within 60 km of the RAOB. Most radiosonde soundings are done at 0Z and 12Z, and imposing too small of an SSM/I-RAOB time window would eliminate many sites. For example, using a 1 hour time window would select only those sites with longitudes near 90E and 90W since the F08 SSM/I has an ascending node time of 6 AM. Thus, we decided to use a 6 hour time window so that all sites are included. We consider that it is more important to have a global distribution of RAOB sites than near simultaneous observations from a few sites. When more than one RAOB observation is within the $\pm$ 6 hour of the SSM/I overpass time, we simply take the RAOB observation that is closest in time, rather than averaging or interpolating the observations.

An objective quality control (Q/C) procedure was used to discard incomplete and anomalous soundings. Each radiosonde sounding consists of a number of levels, with each level containing a measurement of pressure, temperature, and dewpoint depression. If any of these three measurements is missing, the level is discarded. We define the tropospheric RAOB levels as those levels for which the pressure is greater than 180 mb. A cutoff value of 180 mb is used so as to include the mandatory 200 mb level. The first step in the Q/C is to discard the sounding if any of the following conditions occur for any tropospheric level:

1. Air pressure > 1050 mb
2. Air temperature outside –99.9 C to 35 C range
3. Dew point depression outside 0 C to 50 C range
4. Abnormal NCAR quality control flags occur

These conditions occurred for only 0.3% of the soundings.

The next Q/C step was to verify that the sounding contains a valid surface level reading, which is a very important level since much of the water vapor is near the surface. The RAOB data set contains a Q/C flag that identifies the surface level and indicates if it agrees with the surface report. We discarded all soundings that do not have a good quality surface level. This eliminated about 8% of the total soundings. The sounding was also discarded if the first level is less than 940 mb.

The Q/C procedure also discarded soundings that do not go high enough or that are missing too many levels. We required that there be at least 7 tropospheric levels and that the altitude gap between adjacent levels is always less than 3 km. Furthermore, we required that the highest tropospheric level has an air pressure less than 520 mb and a water vapor pressure less than 0.5 mb. These conditions assure that the water vapor profile is adequately sampled. The final Q/C procedure was to discard soundings that display a large discontinuity in temperature or water vapor pressure. This procedure eliminated 2% of the soundings.

Those soundings passing the Q/C test were then extrapolated from the elevation of the radiosonde station down to the sea surface. The sea-surface air pressure and vapor pressure are found by assuming they vary exponential with height, and the sea-surface air temperature is found by assuming it varies linearly with height. The assumed exponential decay rate for vapor pressure is $-0.63$ km$^{-1}$, and the assumed air temperature lapse rate is $-5.8$ C/km. These two values are the global average values for all of the soundings passing the Q/C test. Since all but 3 radiosonde stations are at an elevation less that 100 m, the extrapolation down to the sea surface is a small correction that adds about 3% to the total columnar water vapor.

Another small correction was done to account for the water vapor above the tropospheric level. For the sounding levels in the stratosphere, we did not used the RAOB water vapor measurements because they are not reliable. Instead, we simply assumed an exponential decay rate of $-0.63$ km$^{-1}$ based on the vapor pressure at the highest tropospheric level. This upward extrapolation extends to 50 km and typically adds about 0.2% to the columnar vapor content.

## 4. UPDATED SSM/I-2 OCEAN RETRIEVAL ALGORITHM

We have completed a major update to our algorithm for retrieving geophysical parameters over the world's oceans. Over the past 7 years, the geophysical products from our original algorithm, called SSM/I-1, have been widely distributed to approximately 100 institutions worldwide and have undergone extensive evaluation. These evaluations have revealed small, but significant, problems with the SSM/I-1 products. In addition, with the compilation of the very large *in situ* data sets discussed above, a precise calibration of the algorithm could be performed. Therefore, we decided to update the SSM/I algorithm.

The updated algorithm, called SSM/I-2, has now been completed. In addition to being precisely calibrated to the *in situ* data set, the following problems have been corrected.

1. In very cold areas having low water vapor and low sea surface temperature, the SSM/I-1 winds were biased high by about 1 to 2 m/s. This problem was due to the specified effective air temperature being too high for these cold areas.

2. The SSM/I-1 winds contained an error of 1 to 2 m/s that is correlated with wind direction. This problem was due to the upwind $T_B$ being higher than the downwind $T_B$.

3. For the case of moist air over cold water, the SSM/I-1 water vapors were about 4 mm higher than the radiosonde vapors. For the opposite case of dry air over warm water, the SSM/I-1 vapors were about 4 mm too low. This problem was due to the specified effective air temperature having no dependence on water vapor.

4. There was a relatively large rms error between the SSM/I-1 and radiosonde water vapors. This problem was again due to the specified effective air temperature having no dependence on water vapor.

5. There was an appreciable number of negative cloud water retrievals. This problem was due to the wind direction error mentioned above and to a small decorrelation between the 22 and 37 GHz vapor absorption coefficients.

In response to these problems and to the *in situ* inter-comparisons, the following changes were made to the algorithm's $T_B$ model function.

1. An effective air temperature was derived from radiosonde observations as a function of both the columnar water vapor and the sea surface temperature.

2. The 37H specular emissivity was adjusted to remove the cold-water wind-speed bias.

3. The coefficients for the wind-induced emissivities were adjusted to obtain optimum agreement with the buoy wind speeds.

4. The coefficients for the water vapor absorption were adjusted to obtain optimum agreement with the radiosonde water vapors.

5. The sky radiation that is scattered from the sea surface is more rigorously modeled.

6. The wind-induced emissivities now depend on SST as well as wind speed.

In addition to making these changes to the $T_B$ model function, the estimation procedure was also modified. In SSM/I-1, only the 22 and 37 GHz channels were used. In SSM/I-2, the 19 GHz channels are brought in to play. They are used to mitigate the wind direction error and the error due to the small decorrelation between the 22 and 37 GHz vapor absorption coefficients.

The resulting SSM/I-2 algorithm is extremely well calibrated, and the problems listed above have been corrected. The top row in Figure 2 shows the SSM/I minus buoy wind speed $\Delta W$ plotted versus four parameters: (1) sea surface temperature, (2) wind speed, (3) water vapor, and (4) cloud water. The solid curve is the mean value of $\Delta W$ and the dashed curves are the $\pm$ 1 standard deviation of $\Delta W$. As can be seen, there is no crosstalk between the retrieved wind speed and the four parameters. The $\Delta W$ versus wind plot shows that the retrieved wind speed has the correct dynamic range. The second row in Figure 2 shows analogous results for the SSM/I minus RAOB water vapor $\Delta V$. Again, there is no apparent

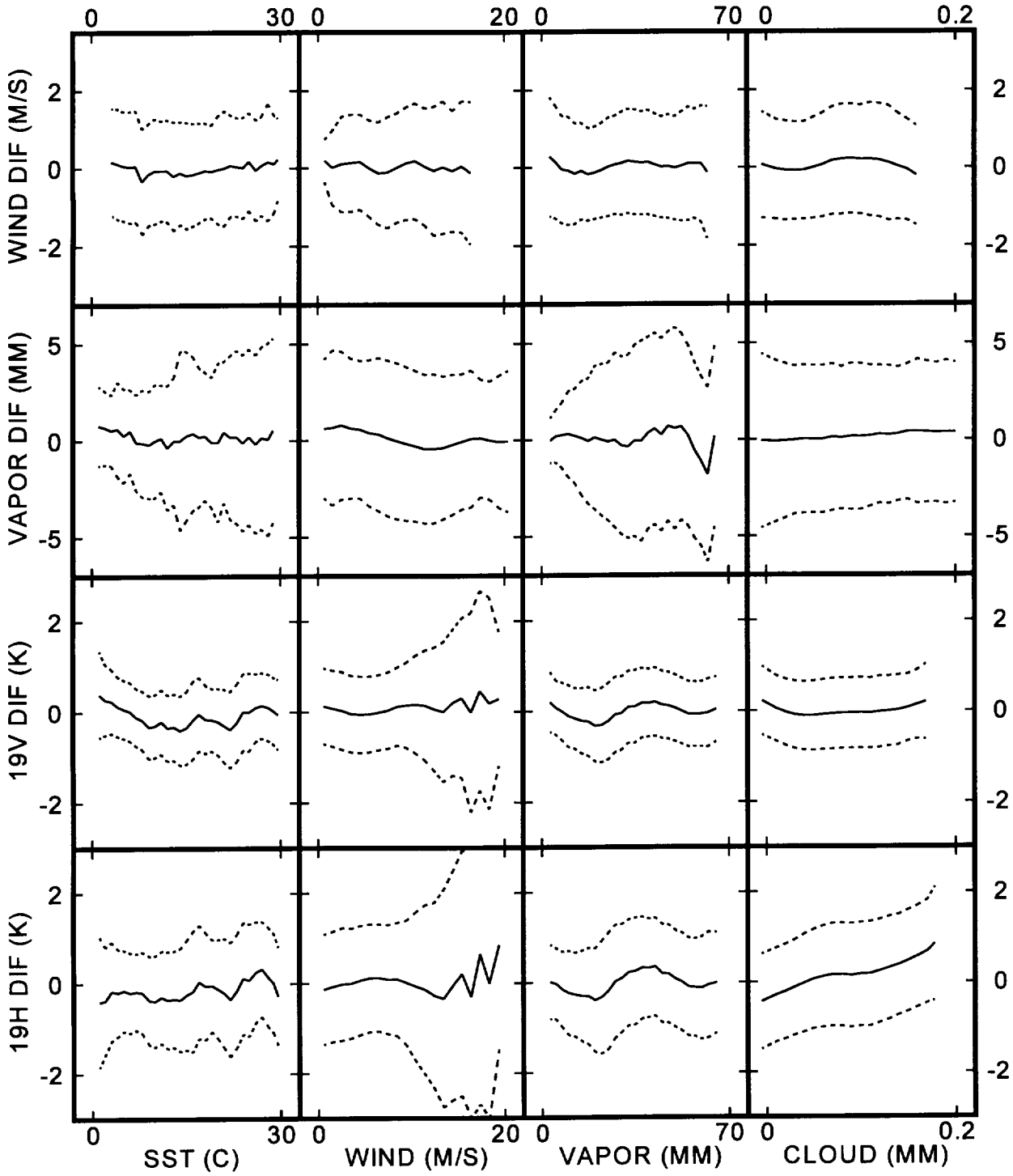


Fig. 2. Results of the SSM/I versus buoy and RAOB intercomparisons. The top row shows the SSM/I minus buoy wind speed difference. The second row shows the SSM/I minus RAOB water vapor difference. The bottom two rows show the SSM/I minus model $T_B$ difference at 19 GHz for v-pol and h-pol. Each column shows the results when stratified according to sea surface temperature, wind speed, water vapor, and cloud water, respectively.

crosstalk in the vapor retrieval, and the retrieved vapor has the correct dynamic range. The rms accuracies of the retrieved wind speed, water vapor and cloud water are approximately 1 m/s, 1 mm, and 0.02 mm, respectively. We know of no other SSM/I algorithm that can match this performance.

## 5. F10 AND F11 OCEAN PRODUCTS FOR 1991 THROUGH 1993

Using the new SSM/I-2 algorithm and the F08-F10-F11 cross-calibration coefficients, we generated ocean products for the F10 and F11 SSM/I's for the years 1991, 1992, and 1993. These products include the near-surface wind speed, atmospheric columnar water vapor, the columnar cloud water, and rain rate. In addition, ocean areas having an ice concentration exceeding about 5% are identified. The SSM/I-2 algorithm is a physical retrieval technique in which the observations are matched to the radiative transfer function. The algorithm simultaneously finds wind speed, water vapor, and liquid water. In addition to the ocean products, data inventory figures and monthly averaged $T_A$ maps were generated. The data inventory figures are a convenient method for displaying time periods of missing data and time periods of erroneous data. The monthly $T_A$ maps will later be used to produce monthly wind vector maps from the SSM/I. Extensive quality control were applied to the generation of the ocean products. These quality control measures include the following:

1. Consistency and out-of-bounds (OOB) checks on the sensor calibration data.
2. Visual inspection of the data inventory figures.
3. OOB checks on the $T_A$'s.
4. Checks on the after-the-fit $T_B$ residual coming from the geophysical algorithm.
5. Exclusion of observations near land or ice.

## 6. THE VARIATION OF THE OCEAN $T_B$ WITH WIND DIRECTION

Several years ago, we detected a wind direction signal in the SSM/I ocean brightness temperatures ($T_B$). This original analysis was based on a limited set of 3000 SSM/I overpasses of buoys in mid-latitudes for a 9-month period. Because of the limited geographical area and time period, there remained the question of whether the detected signal would be the same for all seasons and ocean areas. Now, with the very large SSM/I-buoy data set discussed above, we are able to examine the wind direction signal in more detail.

The SSM/I $T_B$'s were binned according to the relative azimuth angle, which is the angle between the SSM/I azimuth look direction and the wind direction. The statistics were also stratified according to sea surface temperature (SST) and wind speed. Our SSM/I-buoy data covers the full range of conditions from the equator to the arctic ice edge. The results clearly show that $T_B$ varies harmonically with the relative azimuth angle, and that the amplitude of the variation increases approximately linearly with wind speed. Figure 3 shows the variation of the sea-surface brightness temperature versus the relative wind direction for the 4 wind-speed stratifications and the 3 SST stratifications. The displayed quantity is the following linear combination of the v-pol and h-pol $T_B$'s: $2T_{BV} - T_{BH}$. This quantity is insensitive to

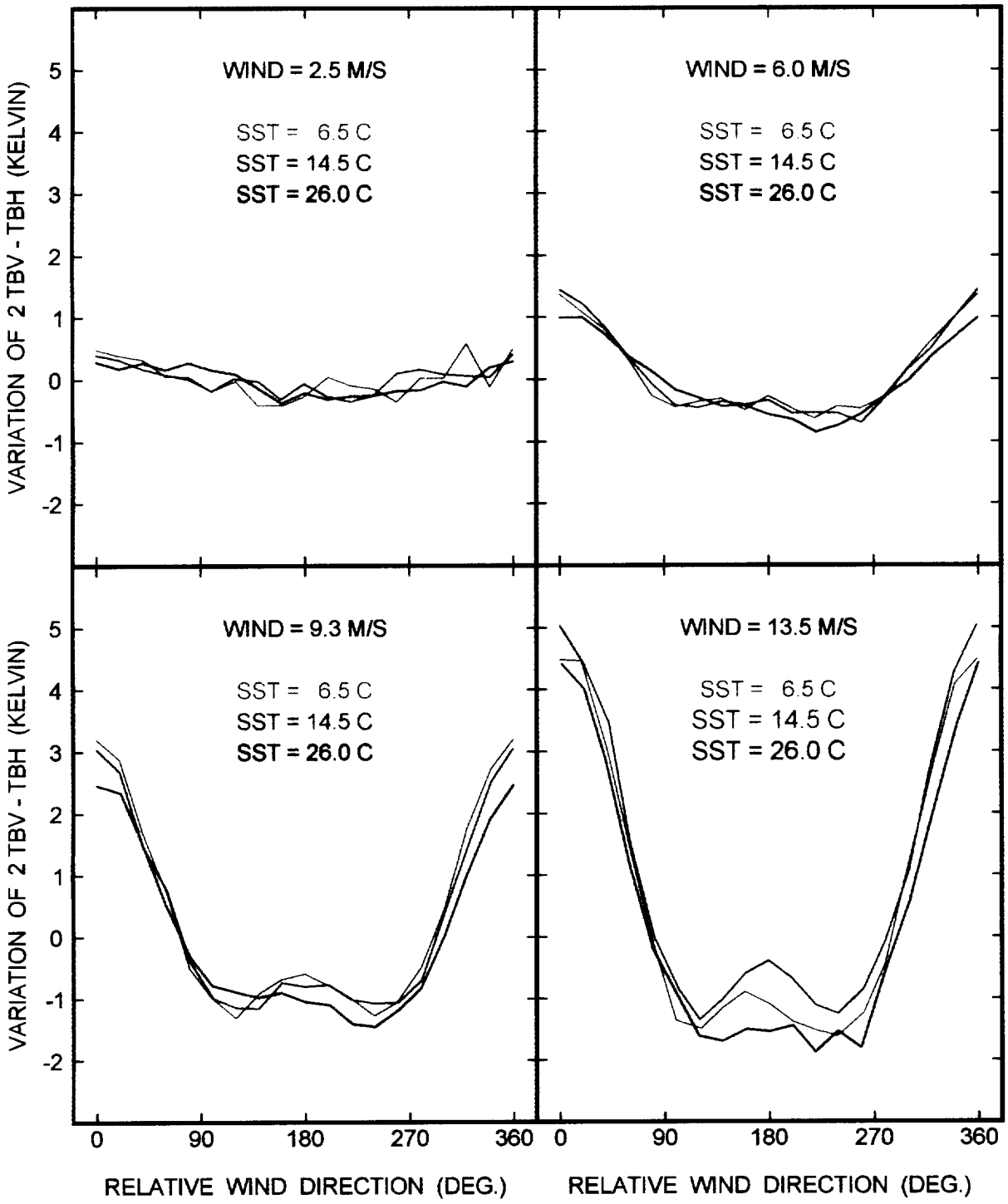


Fig 3. The variation of the sea-surface brightness temperature versus the relative wind direction. Each plot corresponds to a specified wind speed stratification, and each curve corresponds to a specified sea-surface temperature stratification. The displayed quantity is the following linear combination of the v-pol and h-pol $T_B$'s: $2T_{BV} - T_{BH}$.

variations in the atmospheric attenuation. The same wind direction signal is found in the tropics, mid-latitudes, and poleward latitudes, and this signal is in close agreement with that found in the original analysis. These results further support the feasibility of using satellite microwave radiometers for measuring wind direction.

## 7. LINE-OF-SIGHT WIND VECTOR MEASUREMENTS BY SSM/I

We have demonstrated that under high wind conditions, wind direction information can be obtained from individual SSM/I observations. Previously, we had to average many SSM/I orbits to obtain wind direction. However, at the higher wind speed, the upwind-downwind $T_B$ difference is sufficiently large to allow for the determination of the line-of-sight wind vector for individual pixels. This newly found capability is best described via Figure 4, which shows two SSM/I passes over a pair of North Pacific storms just south of the Aleutian Islands. The top row of images shows the rainfall, wind speed, and wind direction signal observed by a descending pass. The bottom row shows the same parameters observed 12 hours later by an ascending pass. The wind direction signal is the change in the ocean surface brightness temperature (K) due to wind direction. For the descending pass, the SSM/I observes the westside of the storm where the winds are blowing from the north. This is a downwind observation, and the wind direction signal is -6 K. The westside of the storm is again observed during the ascending pass, but this time from the upwind direction since SSM/I is now looking north. In this case, the upwind signal is +4 K. The ascending pass also views a second storm coming out of the west. The southerly winds in front of this second storm are seen from the downwind direction and exhibit a -6 K wind direction signal. Further to the west at the top-left corner of the SSM/I swath, the winds shift to westerly. In this area, SSM/I is looking directly into the wind (i.e., upwind), and the wind direction signal is +4 K.

The wind-direction signals shown in Figure 4 are a measure of the line-of-sight wind vector, analogous to Doppler radar measurements. Positive (negative) values indicate the wind is blowing towards (away from) the observer. For the high winds being considered, the signal is quite large, varying by 10 K. Lower winds will exhibit a weaker signal. These results are a further indication that a modified SSM/I, having both forward and aft looks with an additional polarimetric channel, would be an excellent satellite wind vector sensor for future missions. The results also suggest that a single-look (as opposed to two-look) polarmetric radiometer may be able to measure both wind speed and direction for moderate to high winds.

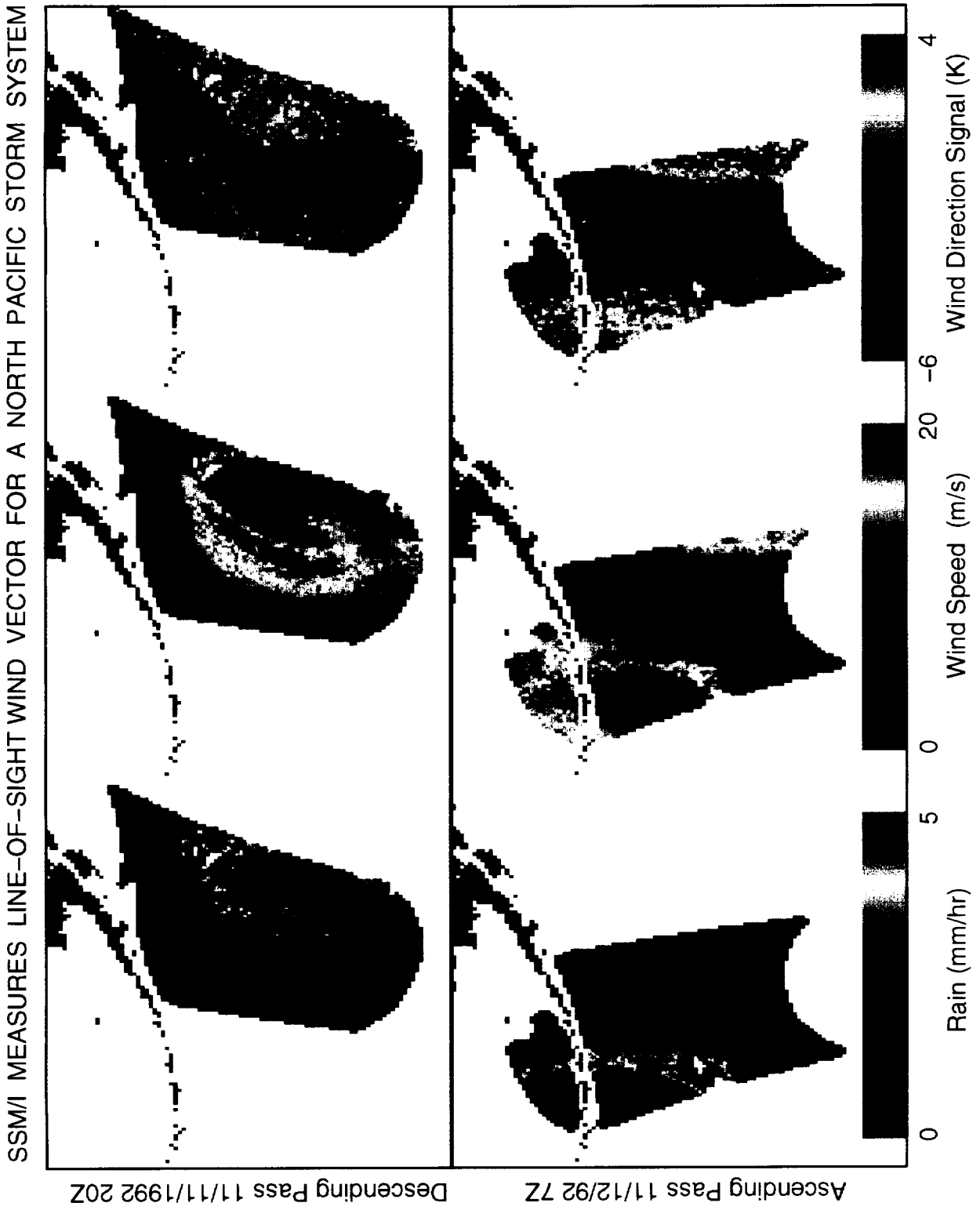


Fig 4. SSM/I observations of rain and line-of-sight wind vector in two North Pacific storms.

## 8. WORK PLANNED FOR NEXT 18-MONTH PERFORMANCE PERIOD

1. The SSM/I-2 algorithm will be used to generate ocean products for the F10 and F11 SSM/I's for the year 1994. These research quality products include wind speed, atmospheric water vapor, cloud water, and rain. In addition, ocean areas having an ice concentration exceeding about 5% will be identified. The algorithm that computes the ocean products is a physical retrieval technique in which the observations are matched to the radiative transfer function. It simultaneously finds wind speed, water vapor, and liquid water.

2. Monthly global wind vector maps will be generated from the SSM/I data. The SSM/I observations will be binned into monthly $5^{\circ}$ latitude by $10^{\circ}$ longitude cells, and then a harmonic analysis will be done to find wind direction. The monthly global wind vector maps will be evaluated by comparing them to ECMWF fields. The zonal and meridional wind components will be analyzed separately. The SSM/I zonal wind component may be more accurate than the meridional component because of the nature of the SSM/I scan geometry. The SSM/I scans east to west during an ascending orbit segment and scans west to east during a descending orbit segment. Variations in the zonal wind speed will be seen as a modulation in the brightness temperatures along each scan. Variations in the meridional component are not as apparent because a given scan does not look north and south. To determine the meridional component, ascending and descending orbits must be combined, and diurnal effects will introduce an error into the computation of the meridional wind.

3. We will conduct simulations of a two-look radiometer. The simulations will be done for a wide variety of conditions in which realistic wind fields will be used. These simulations will be modeled after those done for NASA's NSCAT and SeaWinds scatterometers. The objective of the simulations is to predict, with confidence, the actual performance of a two-look satellite radiometer.

4. This investigation has resulted in a number of interesting and important findings. We now need to publish these results in the scientific literature. We plan to publish the following four papers during the last phase of this investigation:

> *A Well-Calibrated Ocean Algorithm for SSM/I.* This paper will describe the derivation of the SSM/I-2 algorithm along with the buoy and radiosonde data sets that were used to calibrate SSM/I-2. There will also be discussions on the spatial and temporal variability of the wind and vapor fields and retrieval accuracies.
>
> *A Unified, All-Weather Ocean Algorithm for Microwave Radiometers.* This paper will show how the SSM/I-2 algorithm can be combined with a rain retrieval algorithm in a logically consistent manner. The resulting combined algorithm simultaneously finds all of the relevant geophysical parameters for all weather conditions (clear skies, clouds, and rain). Thus, for the first time, a single unified algorithm can be used to simultaneously retrieve wind speed, water vapor, cloud water, and rain rate over the world's oceans.

*The Measurement of Wind Speed and Direction by SSM/I.* This paper will discuss the three components of our SSM/I wind direction analysis. These components are (1) the $T_B$ wind direction signal derived from the collocated buoy and SSM/I observations, (2) the line-of-sight wind vector measurements of SSM/I, and (3) the monthly global wind vector maps.

*The Cross-Calibration of the DMSP SSM/I's.* The technique of cross-calibrating the F08-F10-F11 SSM/I's will be described. We will publish the cross-calibration coefficients so that other investigators can also produce long time series of SSM/I products that are free of inter-satellite biases.

We believe that these papers will represent a significant advancement in the state-of-the-art of microwave radiometry.

5. The principal investigator, F. Wentz, will continue participating in various NASA working groups relevant to SSM/I.